Mixed Convection and Permeability Effects on MHD Williamson Fluid Flow over an Inclined Stretchy Surface with Radiation Influence: Analytical Investigation

R.A. Oderinu[1], T.A. Oyeyinka[1], Saheed Alao[1], F.J. Ayanbukola[1], and B.A Sanusi[1]

[1]Ladoke Akintola University of Technology

November 04, 2024

Abstract

The study introduces a computational method that combines Legendre polynomials with Gauss-Lobatto points to solve nonlinear coupled differential equations, focusing on the Williamson fluid model with the existence of mixed convection and permeability under mixed boundary conditions. The nonlinear governing equations were transformed to ordinary differential equation (ODE) from partial differential equation (PDE), applying the appropriate similarity conversions. By using Legendre polynomials as trial functions and collocating residual equations with Gauss-Lobatto points, the system is solved with Mathematical software. The technique was validated by comparing the obtained solution with an existing literature and further validation was done with Runge-Kutta of order 4 via shooting method. Validation against the Shooting Runge-Kutta method showed minimal discrepancies, confirming the method's accuracy. Graphical analysis indicated that an increase in the Grashof number enhances velocity, while higher porosity raises temperature but reduces fluid velocity. This approach offers an efficient and precise solution for complex nonlinear equations, with broader potential applications in fluid dynamics.

Mixed Convection and Permeability Effects on MHD Williamson Fluid Flow over an Inclined Stretchy Surface with Radiation Influence: Analytical Investigation

R.A. Oderinu, T.A. Oyeyinka, S. Alao*, F.J. Ayanbukola, B.A Sanusi. *

Department of Mathematics, Ladoke Akintola University of Technology, P.M.B 4000, Ogbomoso, Nigeria

Abstract

The study introduces a computational method that combines Legendre polynomials with Gauss-Lobatto points to solve nonlinear coupled differential equations, focusing on the Williamson fluid model with the existence of mixed convection and permeability under mixed boundary conditions. The nonlinear governing equations were transformed to ordinary differential equation (ODE) from partial differential equation (PDE), applying the appropriate similarity conversions. By using Legendre polynomials as trial functions and collocating residual equations with Gauss-Lobatto points, the system is solved with Mathematical software. The technique was validated by comparing the obtained solution with an existing literature and further validation was done with Runge-Kutta of order 4 via shooting method. Validation against the Shooting Runge-Kutta method showed minimal discrepancies, confirming the method's accuracy. Graphical analysis indicated that an increase in the Grashof number enhances velocity, while higher porosity raises temperature but reduces fluid velocity. This approach offers an efficient and precise solution for complex nonlinear equations, with broader potential applications in fluid dynamics.

Keywords: Williamson fluid; Mixed convection; Permeability; Legendre Polynomial; Collocation method.

1 INTRODUCTION

In fluid dynamics, Non-Newtonian fluids are characterized by flow behavior that differs from Newtonian fluids, as their viscosity is not fixed and varies with the application of external forces like shear stress. While Newtonian fluids, such as water and air, maintain a constant viscosity regardless of the stress applied, non-Newtonian fluids display a range of behaviors that depend on the specific conditions under which they are subjected, One particular form of Non-Newtonian fluid is the Williamson fluids, which are of special interest due to their distinctive properties. Unlike typical Newtonian fluids, Williamson fluids exhibit shear-thinning behavior, meaning their viscosity decreases with increasing flow velocity according to Sarkar et al.[1]. This characteristic is particularly important in systems involving complex materials such as blood, polymers, and various industrial substances. Alwawi et al.[2] noted that the practical applications of the Williamson

*Correspondence: salao16@lautech.edu.ng

fluid model extend beyond theoretical considerations, impacting industries like polymer manufacturing, food processing, and medical science, where a deep understanding of blood flow dynamics is critical. There is increasing interest in studying the thermal and mass transfer properties of Williamson fluids. Kebede et al.[3] explored these aspects in the context of unsteady boundary layer flows of Williamson nanofluids, highlighting the need for models that capture the distinct features of these fluids. This is consistent with the earlier work of Nadeem et al.[4], who focused on the flow of Williamson fluids over stretching sheets, setting a foundation for future studies using semi-analytical approaches. Trisaksri and Wongwises [5] conducted a critical evaluation of the heat transfer characteristics of nanofluids. Similarly, Bachok et al. [6] investigated the steady boundary-layer flow of a nanofluid in a uniform free stream over a moving, semi-infinite flat plate.

Recent research has also incorporated various physical effects into Williamson fluid models. Anagandula and Reddy[7] investigate the impact of velocity and thermal slips on Williamson fluid flow over a stretching sheet, accounting for an inclined magnetic field and radiation. Alharbi [8] investigated the influence of thermophoresis and magnetohydrodynamic effects on the behavior of Williamson fluids, emphasizing the complexity of practical applications. Addressing this complexity often requires advanced mathematical techniques, such as those employed by Ahmed et al.[9], who used similarity transformations to simplify nonlinear partial differential equations into ordinary differential equations, making them more amenable to semi-analytical solutions.

The influence of magnetic fields on the flow of Williamson fluids has been a subject of extensive research. Megahed [10] examined the magnetohydrodynamic (MHD) behavior of Williamson fluid over a continuously moving surface, highlighting the significance of viscous dissipation and slip velocity. This study illustrates how the presence of magnetic fields can modify the flow characteristics and thermal properties of non-Newtonian fluids. Similarly, Abbas et al.[11] investigated MHD flow and heat transfer of Williamson nanofluids past a nonlinear stretching sheet, showing that magnetic fields can enhance heat transfer through mechanisms like induced convection and viscous dissipation. Furthermore, Bibi et al. [12] reported substantial alterations in both the velocity profile and temperature distribution within the fluid due to the influence of magnetic fields. Srinivasulu and Goud [13] also investigated the effects of an inclined magnetic field on the flow, heat transfer, and transport phenomena of a Williamson nanofluid passing over a stretching sheet.

Thermal effects, particularly those related to thermal radiation, are crucial in the dynamics of Williamson fluids. Reddy et al.[14] studied the irreversibility of radiative heat transport in Williamson materials, revealing that thermal radiation can have a significant impact on heat transfer and flow behavior. This notion is further supported by Hayat et al.[15], who explored the combined effects of thermal radiation and viscous dissipation in the flow of Williamson fluids over an unsteady stretching surface. Their research indicated that thermal radiation can enhance the temperature field, consequently improving overall heat transfer efficiency. The interplay between thermal and velocity effects in Williamson fluids is also vital. Akolade et al.[16] addressed the influences of thermophoresis and heat sources on Williamson fluid flow, stressing the importance of temperature-dependent properties in their analysis. Their findings demonstrate how variations in temperature can lead to changes in viscosity and thermal conductivity, subsequently affecting flow dynamics and heat transfer rates. Additionally, Choudhari [17] stated that, in mixed convection scenarios where both natural and forced convection are present, complex flow patterns and enhanced heat transfer performance can arise.

Semi-analytical methods have garnered considerable attention in fluid dynamics, particularly for the analysis of Williamson fluids. These methods are valued for their ability to handle complex boundary conditions and the nonlinearities inherent in non-Newtonian fluid behavior.

Recent research highlights the effectiveness of semi-analytical approaches in solving the nonlinear differential equations governing Williamson fluids. Araujo et al.[18] introduced a semi-analytical technique for fluid flows, demonstrating its superiority over traditional numerical methods. However, their focus on the linear Phan-Thien-Tanner fluid model may limit the applicability of their findings to Williamson fluids. Similarly, Karabut et al. [19] found that combining semi-analytical methods with techniques such as Padé approximants can enhance accuracy compared to purely numerical approaches, although they also noted challenges related to complexity and reliability. Additionally, recent developments in semi-analytical techniques, especially the Differential Transform Method (DTM) and Adomian Decomposition Method (ADM), have greatly advanced the study of non-linear differential equations. These approaches not only simplify the process of deriving analytical solutions but also deepen the comprehension of complex systems across numerous scientific fields. Current research in this domain continues to investigate novel combinations of these techniques, broadening the range of tools available to both mathematicians and engineers. (see ref. 20-29)

Kelil and Appadu [30] examined the connection between semi-classical orthogonal polynomials and modified weight functions, highlighting how perturbations in orthogonality measures can lead to novel mathematical insights. Their work underscores the importance of integrating orthogonal polynomials, such as Legendre polynomials, to enhance the accuracy of semi-analytical methods. Additionally, the Gauss-Lobatto collocation technique, a key tool for discretizing differential equations, has proven effective in solving boundary value problems, with successful applications in studies involving nanofluids and magnetohydrodynamic (MHD) flows.

This study indicates that semi-analytical methods, particularly when combined with polynomial basis functions like Legendre polynomials and Gauss-Lobatto collocation points, offer significant potential for enhancing the accuracy and efficiency of solutions. By integrating these techniques, researchers can develop more comprehensive models that effectively capture the complex behaviors of Williamson fluids across diverse practical scenarios.

2 FORMULATIONS OF THE MODEL

In this research, we explore the steady, two-dimensional, laminar flow of a Williamson fluid between two parallel, permeable porous walls. The governing equations for the fluid dynamics are derived by building on the foundational work of Anagandula and Reddy [7]. Specifically, the momentum equation is modified to include the effects of mixed convection, allowing for the influence of both temperature and concentration gradients on the flow. The energy equation is further modified to incorporate the influence of permeability within the porous medium, capturing the heat transfer characteristics of the system. Moreover, the concentration equation is adapted from the work of Alao et al. [34], reflecting the diffusion and reaction phenomena within the flow. This comprehensive model integrates the complexities of fluid mechanics, heat transfer, and mass diffusion to describe the attribute of non-Newtonian Williamson fluid flow under the influence of various forces and physical factors. Fig. 1 shows the flow model for the problem by Anagandula and Reddy[7]

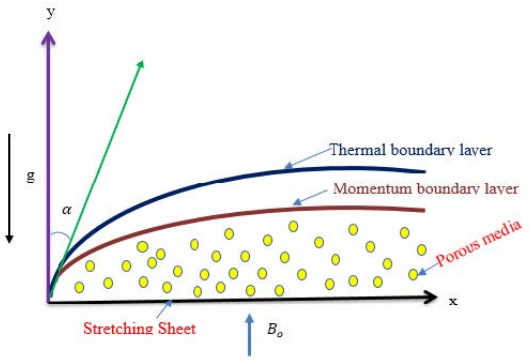

Fig. 1 Flow geometry

$$\frac{\partial u}{\partial x}+\frac{\partial v}{\partial y}=0, \tag{1}$$

$$u\frac{\partial u}{\partial x}+v\frac{\partial u}{\partial y}=\nu\frac{\partial^2 v}{\partial y^2}+\sqrt{2}\nu\Gamma\frac{\partial u}{\partial y}\frac{\partial^2 u}{\partial y^2}-\frac{\sigma B_0^2}{\rho_f}sin^2(\alpha)u-\frac{\nu}{K^*}u+gB_t(T-T_\infty)+$$
$$gB_c(C-C_\infty),\ \text{(Momentum Equation)} \tag{2}$$

$$u\frac{\partial T}{\partial x}+v\frac{\partial T}{\partial y}=\frac{k}{(\rho C_p)_f}\frac{\partial^2 T}{\partial y^2}+\frac{1}{(\rho C_p)_f}\frac{16\sigma^* T_\infty^3}{3K^*}\frac{\partial^2 T}{\partial y^2}+\frac{\sigma\beta_0^2}{(\rho C_p)_f}u^2+\frac{\nu}{C_p}\left[\left(\frac{\partial u}{\partial y}\right)^2+\sqrt{2}\Gamma\left(\frac{\partial u}{\partial y}\right)^3\right]+$$
$$Q_0(T-T_\infty)+\frac{\nu}{\rho C_p K^*}u^2,\ \text{(Energy Equation)} \tag{3}$$

$$u\frac{\partial C}{\partial x}=-v\frac{\partial C}{\partial y}+D\frac{\partial^2 C}{\partial^2 y}-K_n(C-C_\infty),\ \text{(Concentration Equation)} \tag{4}$$

The associated boundary conditions with the governing equations (1) to (4) given in the work of Anagandula and Reddy [7] as:

$$\left.\begin{aligned} u_w=u=ax+A^*\frac{\partial u}{\partial y}, v=v_w, T=T_f+B^*\frac{\partial T}{\partial y}, C=C_f+X^*\frac{\partial C}{\partial y}\text{as y}\to 0,\\ u=0, T=T_\infty, C=C_\infty\text{as y}\to\infty\end{aligned}\right\} \tag{5}$$

Similarity variables is given as follows:

$$\left.\begin{aligned} \eta=y\sqrt{\frac{a}{\nu}},\quad u=axf'(\eta),\quad v=-\sqrt{a\nu}f(\eta),\\ \bar{\theta}(\eta)=\frac{T-T_\infty}{T_w-T_\infty},\quad \bar{\phi}(\eta)=\frac{C-C_\infty}{C_w-C_\infty}.\end{aligned}\right\} \tag{6}$$

By using equation (6), the formulated equations (2)-(5) are now reduced to dimensionless form:

$$(1+\lambda\bar{f}'')\bar{f}'''+\bar{f}\bar{f}''-(\bar{f}')^2-(Msin^2(\alpha)+K_p)\bar{f}'+Gr\theta+Gm\bar{\phi}=0, \tag{7}$$

$$\bar{\theta}''+\frac{Pr}{(1+R)}\left[\bar{f}\bar{\theta}'+Ec\left((\bar{f}'')^2+We(\bar{f}'')^3+M\bar{f}'^2+K_p\bar{f}'^2\right)+Q\bar{\theta}\right]=0, \tag{8}$$

$$\bar{\phi}''+Le\left(\bar{f}\bar{\phi}'-Kn\phi\right)=0. \tag{9}$$

Upon transformtion, the boundary conditions are given as:

$$\left.\begin{aligned}\bar{f}(\eta)=\bar{f}_w, \bar{f}'(\eta)=1+A\bar{f}''(0), \bar{\theta}(0)=1+\delta\bar{\theta}'(0), \bar{\phi}(0)=1+\beta\bar{\phi}'(0) \text{ as } \eta\to 0\\ \bar{f}'(\eta)\to 0, \bar{\theta}(\eta)\to 0, \bar{\phi}(\eta)\to 0, \text{ as } \eta\to\infty\end{aligned}\right\} \quad (10)$$

where, $M=\frac{\sigma B_0^2}{\rho_f a}$ Magnetic term, $\lambda=\sqrt{\frac{2a}{\nu}}ax\Gamma$ Williamson factor, $R=\frac{16\sigma T_\infty^3}{3kk^*}$ Radiative term, $We=x\Gamma\sqrt{\frac{2a^3}{\nu}}$ Weinnesberg parameter, $Pr=\frac{k}{\rho C p_f}$ Prandtl number, $Ec=\frac{u_w^2}{C_p(T_f-T_\infty)}$ Eckert number, $Le=\frac{\nu}{D_a}$ Schmidt number, $\bar{f}_w=\frac{v_w}{\sqrt{a\nu}}$ Suction/Injection constraint, $A=A^*\sqrt{\frac{a}{\nu}}$ Velocity Slip, $\delta=B^*\sqrt{\frac{a}{\nu}}$ Thermal slip, $\beta=X^*\sqrt{\frac{a}{\nu}}$ Mass Slip $Gr=\frac{ag\beta_t(T_w-T_\infty)}{U_w}$ Grasshof number, $Gm=\frac{ag\beta_c(C_w-C_\infty)}{U_w}$ Modified Grasshof number,$K_p=\frac{\nu}{ak^*}$ Permeability factor, $Q=\frac{Q_o}{\rho C_p}$ Heat Source

The local skin friction C_{fx} using (6) is given as:

$$C_{fx}=\frac{\tau_w}{\rho u_w^2}=\left(1+\frac{\lambda}{2}f''(0)\right)f''(0), \quad (11)$$

where the shear stress is defined as:

$$\tau_w=\left[\frac{\partial u}{\partial y}+\frac{\Gamma}{\sqrt{2}}\left(\frac{\partial u}{\partial y}\right)^2\right]_{y=0}, \text{and the thermal flux } q_w(x)=-k\left(\frac{\partial T}{\partial y}\right)_{y=0}. \quad (12)$$

From the similarity variables in (6), solving for the Nusselt number, $Nu_x=\frac{xq_w}{k(T-T_w)}$

$$Nu_x=-(1+R)\theta'(0) \quad (13)$$

3 NUMERICAL APPROACH

The analytical approach employed to solve equations (7) - (9) is the Legendre polynomial in conjunction with shifted Gauss-Lobatto points as collocation points. This technique utilizes interpolation over discrete sub-intervals, selecting a trial function, typically in the form of an exponential or polynomial, to approximate the solution of a differential equation within the integral range $a\le x\le b$. This trial function is then used to determine the coefficients by solving a system of equations at selected nodes. The functions $\bar{f}$, $\bar{\theta}$, and $\bar{\phi}$ are used as trial functions in this process as follows:

$$\bar{f}=LegendreP\sum_{k=0}^{n}a_k\left(\frac{2\eta}{\eta_\infty}-1\right) \quad (14)$$

$$\bar{\theta}=LegendreP\sum_{k=0}^{n}b_k\left(\frac{2\eta}{\eta_\infty}-1\right) \quad (15)$$

$$\bar{\phi}=LegendreP\sum_{k=0}^{n}c_k\left(\frac{2\eta}{\eta_\infty}-1\right) \quad (16)$$

In this approach, a_k, b_k, and c_k, where $k=0,1,2,\ldots,n$, represent the unknown coefficients to be determined, with n denoting the point of convergence of the solution. The transformed boundary conditions (10) are applied to the base functions (14)-(16) to form a system of algebraic

equations. The residuals, $\bar{f}_{res}$, $\bar{\theta}_{res}$, and $\bar{\phi}_{res}$, are then formulated by substituting (14)-(16) into (7)-(9) and collocating at Gauss-Lobatto nodes. These coefficients $[a_k, b_k, c_k \mid k = 0, 1, \ldots, n]$ are expressed as polynomials that minimize the residual error. Using the Mathematica software 11.0, the unknowns are substituted into the trial functions (14)-(16), transforming equations (7)-(9) into:

$$\bar{f}(\eta) = 0.646963+0.139541(-2+\eta)-0.0228544(8-12\eta+3\eta^2)+0.00418138(-16+48\eta-30\eta^2)-$$
$$0.00012927(128-640\eta+720\eta^2-280\eta^3+35\eta^4)+...+$$
$$1.48034\times10^{-21}(274877906944-28862180229120\eta+7540244585760\eta^2-867128127258624\eta^3+$$
$$55279418112737280\eta^4-22111767245094912\eta^5+5988603628879870\eta^6-1154944985569689\eta^7+$$
$$598860362887987200\eta^8-176383091256852480\eta^9+...+25519280463600\eta^{18}+1378465288200^{19}+$$
$$34461632205\eta^{20}) \quad (17)$$

$$\bar{\theta}(\eta) = 0.115522-0.136023(-2+\eta)+0.0347857(8-12\eta+3\eta^2)-0.0113605(-16+48\eta-30\eta^2+5\eta^3)+$$
$$0.000572607(128-640\eta+720\eta^2-280\eta^3+35\eta^4)+...+$$
$$5.90009\times10^{-19}(274877906944-28862180229120\eta+754024458485760\eta^2-867128128127258624\eta^3+$$
$$55279418112737280\eta^4-222111767245094912\eta^5+59886036288798700\eta^6-115494498556968960\eta^7+$$
$$598860362887987200\eta^8-176383091256852480\eta^9+...+25519280463600\eta^{18}+1378465288200^{19}+$$
$$34461632205\eta^{20}) \quad (18)$$

$$\bar{\phi}(\eta) = 0.192086-0.17183(-2+\eta)+0.0268998(8-12\eta+3\eta^2)-0.00490243(-16+48\eta-30\eta^2+5\eta^3)+$$
$$0.000121942(128-640\eta+720\eta^2-280\eta^3+35\eta^4)+...+$$
$$1.16334\times10^{-22}(274877906944-28862180229120\eta+754024458485760\eta^2-867128128127258624\eta^3+$$
$$55279418112737280\eta^4-222111767245094912\eta^5+59886036288798700\eta^6-115494498556968960\eta^7+$$
$$598860362887987200\eta^8-176383091256852480\eta^9+...+25519280463600\eta^{18}+1378465288200^{19}+$$
$$34461632205\eta^{20}) \quad (19)$$

The procedures are iterated for varying the values of thermo-physical parameters. With $Pr = 7$, $Ec = 0.2$, $We = 3$, $Q = 0.2$, $\lambda = 0.2$, $\delta = 0.1$, $R = 0.2$, Table 1 and Table 2 demonstrates the accuracy of Legendre collocation method compared to the existing findings.

Table 1:Comparing the values of Nusselt number, $-\theta'(0)$ with previous results when $\lambda = R = Ec = M = Kp = \alpha = f_w = A = Q = \delta = 0$

Pr	**Wang [31]**	**Gorla and Sidawi[32]**	**Khan and Pop[33]**	**Anagandula and Reddy[7]**	**Present Study**
0.7	0.4539	0.4539	0.4539	0.4539	0.4544
2	0.9114	0.9114	0.9113	0.9113	0.9114
7	1.8954	1.8954	1.8954	1.8954	1.8954

Table 2: The quantities of $Nu_x(Re_x)^{-1/2} = -(1+R)\theta'(0)$, Nusset number with various values of M, f_w, Kp, A, and α and $Gr = Gm = Le = Kn = 0$

M	f_w	**Kp**	**A**	α	**Anagandula and Reddy[7]**	**Present Study**
1	0.1	0.1	0.1	$\pi/6$	1.909836	1.909831
2	0.1	0.1	0.1	$\pi/6$	1.736706	1.736705
3	0.1	0.1	0.1	$\pi/6$	1.602261	1.602256
1	0.3	0.1	0.1	$\pi/6$	2.832506	2.832502
1	0.5	0.1	0.1	$\pi/6$	3.692629	3.692624
1	0.1	0.3	0.1	$\pi/6$	2.014749	2.014745
1	0.1	0.5	0.1	$\pi/6$	2.118347	2.118363
1	0.1	0.1	0.3	$\pi/6$	1.481884	1.481878
1	0.1	0.1	0.5	$\pi/6$	1.268373	1.268369

Table 3: Comparing Outputs of Skin Friction $\left(1+\frac{\lambda}{2}f''(0)\right)f''(0)$ with varying Gr, M, f_w, and Kp; other values are $R = 0.2$, $Kn = 0.5$, $Le = 1$, $\beta = 0.2$, $\alpha = \frac{\pi}{6}$, $A = 0.5$ using Shooting Runge-Kutta Method (SRK) and Legendre Collocation Method (LCM)

Gr	Gm	M	f_w	Kp	**SRK**	**LCM**
0.5	0.1	1.0	0.1	0.1	-0.620668	-0.622017
1.0	0.1	1.0	0.1	0.1	-0.524751	-0.526129
1.5	0.1	1.0	0.1	0.1	-0.438566	-0.440006
0.5	0.5	1.0	0.1	0.1	-0.517852	-0.519804
0.5	1.0	1.0	0.1	0.1	-0.403309	-0.405426
0.5	0.1	2.0	0.1	0.1	-0.666787	-0.667241
0.5	0.1	3.0	0.1	0.1	-0.708830	-0.709621
0.5	0.1	1.0	0.3	0.1	-0.702310	-0.705824
0.5	0.1	1.0	0.5	0.1	-0.777817	-0.779436
0.5	0.1	1.0	0.1	0.3	-0.664450	-0.666721
0.5	0.1	1.0	0.1	0.5	-0.704115	-0.705812

Table 4: Comparing Outputs of Nusselt Number $(1+R)\theta'(0)$ varying Kp, Pr, Ec, We, and R; other values remain the same using Shooting Runge-Kutta Method (SRK) and Legendre Collocation Method (LCM)

Kp	Pr	Ec	We	R	**SRK**	**LCM**
0.5	3	0.2	3	0.2	-0.618327	-0.618425
1.0	3	0.2	3	0.2	-0.502557	-0.502621
1.5	3	0.2	3	0.2	-0.391398	-0.391543
0.5	5	0.2	3	0.2	-0.923485	-0.923643
0.5	7	0.2	3	0.2	-1.181955	-1.182359
0.5	3	0.4	3	0.2	-0.446266	-0.446514
0.5	3	0.6	3	0.2	-0.256102	-0.256372
0.5	3	0.2	4	0.2	-0.664453	-0.664684
0.5	3	0.2	5	0.2	-0.711120	-0.711352
0.5	3	0.2	3	0.3	-0.627211	-0.627413
0.5	3	0.2	3	0.4	-0.635129	-0.635482

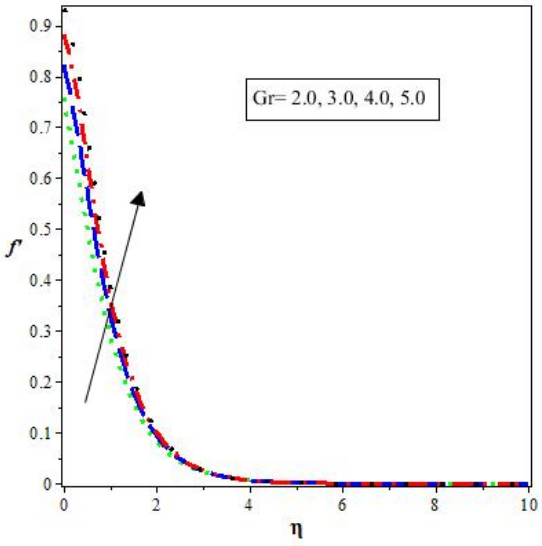

Fig. 2: Effect of varying Gr on $f'(\eta)$.

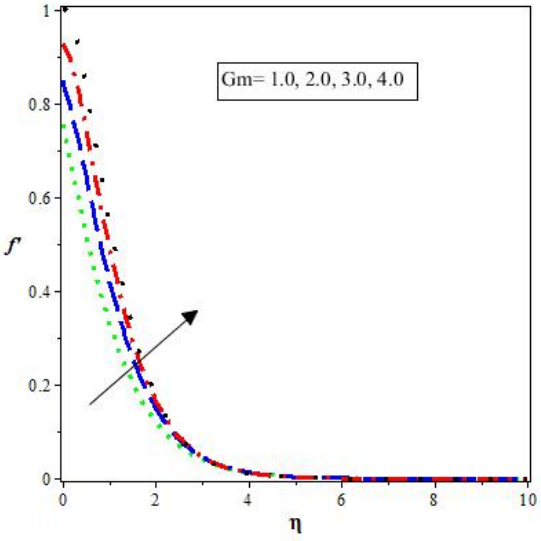

Fig. 3: Effect of varying Gm on $f'(\eta)$.

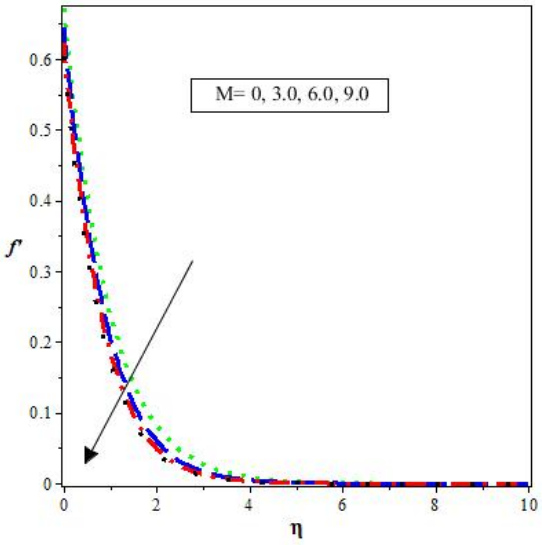

Fig. 4: Influence of varying M on $f'(\eta)$.

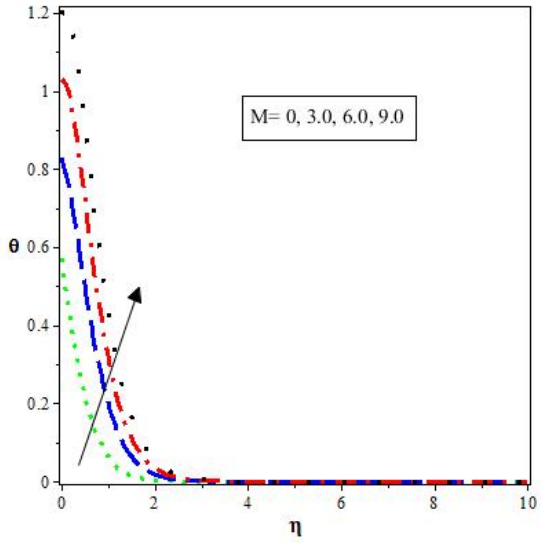

Fig. 5: Influence of varying M on $\theta(\eta)$.

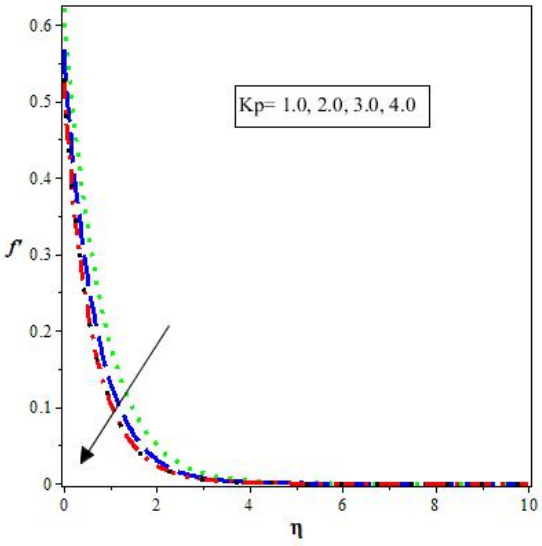

Fig. 6: Impact of varying Kp on $f'(\eta)$.

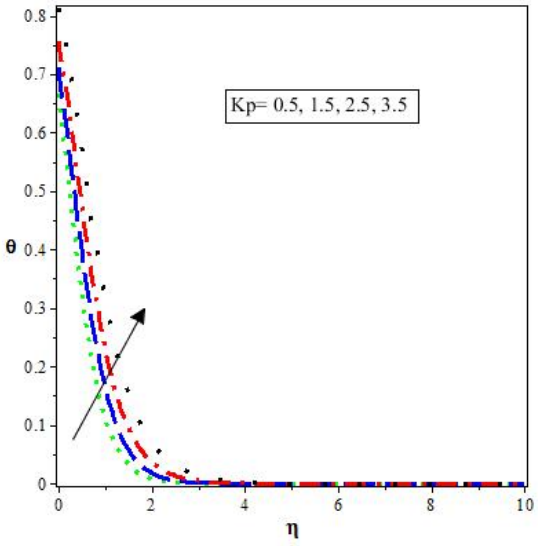

Fig. 7: Impact of varying Kp on $\theta(\eta)$.

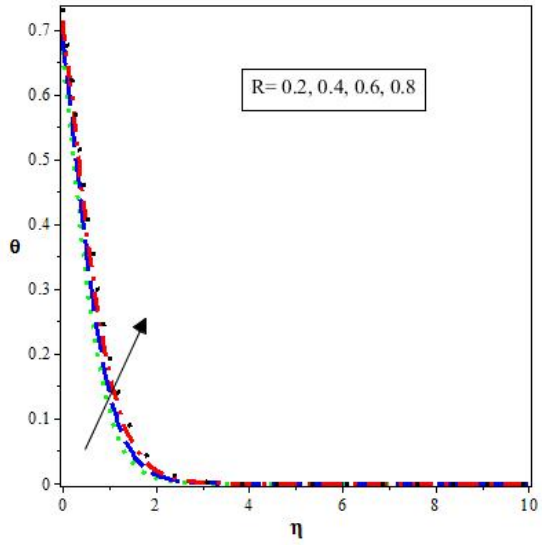

Fig. 8: Influence of R against $\theta(\eta)$.

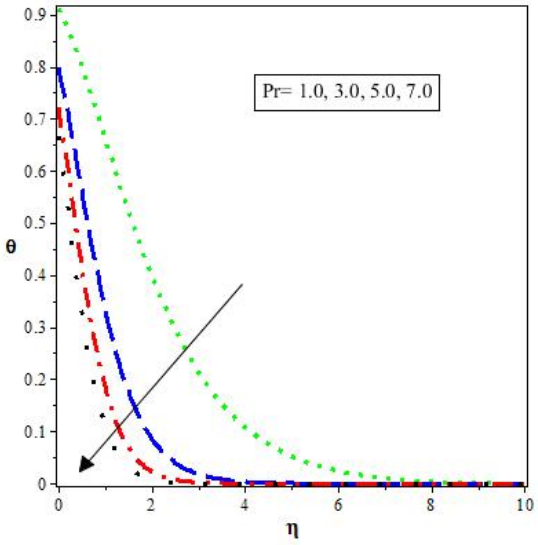

Fig. 9: Influence of Pr against $\theta(\eta)$.

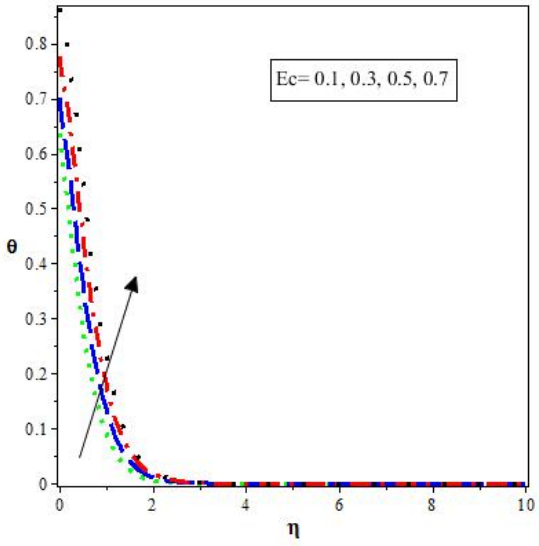

Fig. 10: Effect of varying Ec on $\theta(\eta)$.

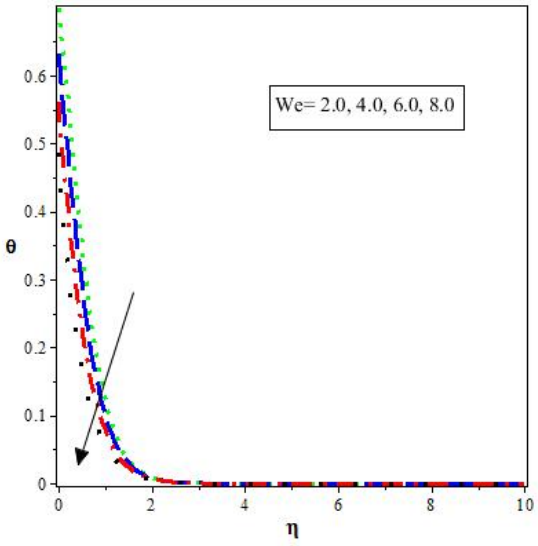

Fig. 11: Effect of varying We on $\theta(\eta)$.

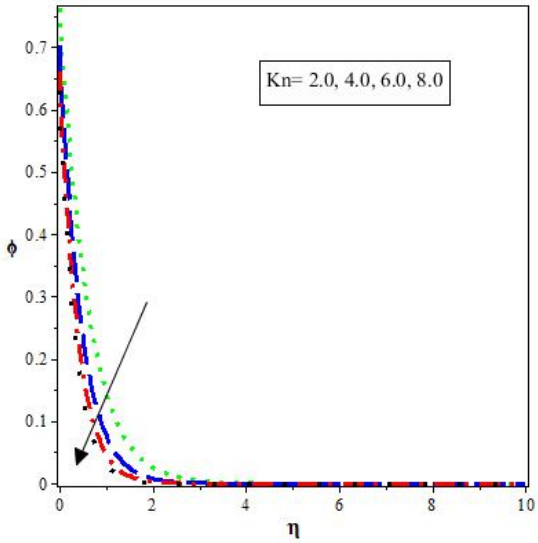

Fig. 12: Kn against $\phi(\eta)$.

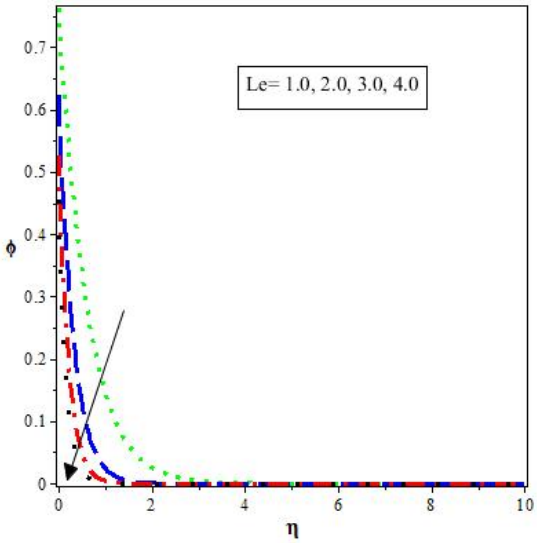

Fig. 13: Le against $\phi(\eta)$.

4 DISCUSSION OF RESULTS

This study effectively derived approximate solutions for the non-linear modified coupled system of equations (7)-(9) by applying the Legendre collocation method and utilizing the fourth-order Runge-Kutta technique with the shooting method as a control method. The impact of the physical parameters on velocity, temperature, and concentration distributions is illustrated through the results, which are presented in Tables 3 and 4 and Figures 2-13.

Tables 3 and 4 illustrate the computed values for skin friction and the Nusselt number respectively. The tables compare the results obtained using the shooting method with the Runge-Kutta approach against the present study, further demonstrating the credibility and effectiveness of the proposed method.

The graphs correspond to the solutions of (7)-(9), which are subject to the boundary conditions given in (10), Figure 2 illustrates how changes in the Grashof number (Gr) impact the

velocity profile. As the Grashof number increases, it indicates that buoyancy forces within the fluid are becoming stronger compared to the resisting viscous forces. This increase in buoyancy leads to more active fluid movement, resulting in a faster flow. With higher Grashof numbers, heat convection plays a more significant role, contributing to greater circulation and mixing, which in turn raises the velocity.

Similarly, Figure 3 presents the effects of the modified Grashof number (Gm) on the velocity profile. As Gm increases, buoyancy starts to dominate over viscosity, encouraging more fluid circulation and leading to a noticeable rise in velocity.

Figures 4 and 5, shows the effect of magnetic factor (M) on velocity and temperature profiles respectively. It is noticeable that as M increases, there is a corresponding increase in temperature, in contrast, the influence of the magnetic field on velocity suppresses the movement of the fluid, This is because the magnetic field introduces a resistive effect, usually described as the Lorentz force, a drag force, similar to friction, that opposes the movement of the fluid particles.

Figures 6 and 7 demonstrate the variance in velocity and temperature profiles, in relation to the porosity term Kp. It is evident that as the porosity factor rises, an associated increase is seen in temperature, while velocity decreases. This indicates that higher porosity enhances heat retention within the medium but reduces fluid flow due to the greater resistance to movement through the porous structure.

The increase in the radiation factor shown in Figure 8 corresponds to a decrease in the temperature profile. This suggests that as radiation increases, it effectively enhances heat loss from the fluid, leading to lower temperatures within the system.

Figure 9 illustrates the manner with which the Prandtl number (Pr) influences the temperature profile of the fluid. As the Prandtl number goes up, the fluid's ability to conduct heat decreases. This means that heat doesn't spread through the fluid as quickly, causing it to take longer to penetrate and distribute evenly. As a result, there is steeper temperature differences near the heated surface, highlighting how the fluid's thermal behavior changes with varying Prandtl numbers.

Figure 10 demonstrates the impact of the Eckert number on the thermal distribution. It is observed that an increase in the viscous dissipation parameter (Ec) results in a rise in the temperature profile. This occurs because the frictional heating generated by fluid motion causes heat energy to be retained within the liquid, thus increasing its temperature.

The outcome of a rise in the Weinnesberg parameter in figure 11, depicts a noticeable reduction in the temperature profile, implying that with a rise in the parameter, the fluid's viscosity decreases under shear stress. Similarly, Figure 12 highlights the impact of the chemical reaction term (Kn) on the concentration profile. As the chemical reaction term increases, the concentration decreases. This happens because the reaction reduces the thickness of the concentration boundary layer, making it harder for mass to accumulate, thus lowering the concentration.

Figure 13 demonstrates how the Schmidt parameter (Le) impacts the concentration profile. As the Schmidt number increases, the ability of the fluid to diffuse mass decreases, which in turn reduces the overall mass transfer and lowers the concentration in the fluid.

5 CONCLUSION

This research focused on applying Legendre polynomials and Gauss-Lobatto points to solve differential equations arising from the Williamson fluid model under mixed boundary conditions. The study involved formulating an appropriate model to examine the effects of mixed convection, porosity, and concentration. By using similarity variables, the independent variables were

reduced from partial differential equations (PDEs) to ordinary differential equations (ODEs), and numerical methods were employed to analyze the behavior of various thermophysical parameters. The results were compared with the existing work using the Shooting RK-4 method as a control and the Legendre collocation method for verification. The findings showed consistency with established literature Anagandula and Reddy [7]. It was observed that:

- As the Grashof number increased, the velocity profile enhanced.
- An increase in porosity led to a rise in temperature, while the velocity decreased. This suggests that higher porosity improves heat retention in the medium but reduces fluid flow due to increased resistance through the porous structure.
- An increase in the magnetic parameter results in higher skin friction values at the lower wall, while the upper wall exhibits a decrease in skin friction.
- An increase in the radiation parameter R and the Eckert number Ec leads to a rise in temperature.

This study successfully developed a mathematical model to analyze the combined effects of key parameters such as the Grashof number, modified Grashof number, porosity, Schmidt number, and chemical reactions on the behavior of Williamson fluid dynamics. By employing a novel computational approach using Legendre polynomials as basis functions, an innovative solution to the nonlinear Williamson fluid model was achieved. The results of this research provide valuable insights into the impact of these parameters on fluid flow. It is recommended that future studies consider incorporating nanoparticles into the model to enhance thermal energy transfer, offering further optimization of fluid flow dynamics and a deeper understanding of the thermal properties involved in Williamson fluids.

References

[1] T. Sarkar, S. Reza-E-Rabbi, S. Arifuzzaman, R. Ahmed, M. Khan, & S. Ahmmed. (2019). Mhd radiative flow of casson and williamson nanofluids over an inclined cylindrical surface with chemical reaction effects. *International Journal of Heat and Technology*, 37(4), 1117-1126. https://doi.org/10.18280/ijht.370421

[2] F. Alwawi, F. Faqih, M. Swalmeh, & M. Ibrahim. (2022). Combined convective energy transmission performance of williamson hybrid nanofluid over a cylindrical shape with magnetic and radiation impressions. *Mathematics*, 10(17), 3191. https://doi.org/10.3390/math10173191

[3] T. Kebede, E. Haile, G. Awgichew, & T. Walelign. (2020). Heat and mass transfer in unsteady boundary layer flow of Williamson nanofluids. *Journal of Applied Mathematics*, 2020, 1-13. https://doi.org/10.1155/2020/1890972

[4] S. Nadeem, S. Hussain, & C. Lee. (2013). Flow of a williamson fluid over a stretching sheet. *Brazilian Journal of Chemical Engineering*, 30(3), 619-625. https://doi.org/10.1590/s0104-66322013000300019

[5] V. Trisaksri & S. Wongwises. (2007). Critical review of heat transfer characteristics of nanofluids. *Renewable and Sustainable Energy Reviews*, 11(3), 512-523. https://doi.org/10.1016/j.rser.2005.01.010

[6] N. Bachok, A. Ishak, & I. Pop. (2010). Boundary-layer flow of nanofluids over a moving surface in a flowing fluid. *International Journal of Thermal Sciences*, 49(9), 1663-1668. https://doi.org/10.1016/j.ijthermalsci.2010.01.026

[7] S. Anagandula & K. S. Reddy. (2024). Velocity and thermal slips impact on the williamson fluid flow above a stretching sheet in the existence of radiation and inclined magnetic field. *CFD Letters*, 16(7), 118-135. https://doi.org/10.37934/cfdl.16.7.118135

[8] L. Alharbi. (2024). Analyzing the impact of thermophoresis particle deposition and magnetohydrodynamic cross-flow of Williamson hybrid nanofluids across a permeable deformable surface. *ZAMM - Journal of Applied Mathematics and Mechanics*, 104(7). https://doi.org/10.1002/zamm.202300947

[9] K. Ahmed, T. Akbar, & T. Muhammad. (2021). Physical aspects of homogeneous-heterogeneous reactions on MHD Williamson fluid flow across a nonlinear stretching curved surface together with convective boundary conditions. *Mathematical Problems in Engineering*, 2021, 1-13. https://doi.org/10.1155/2021/7016961

[10] A. Megahed. (2019). Steady flow of mhd williamson fluid due to a continuously moving surface with viscous dissipation and slip velocity. *International Journal of Modern Physics C*, 31(01), 2050019. https://doi.org/10.1142/s0129183120500199

[11] A. Abbas, M. Jeelani, A. Alnahdi, & A. Ilyas. (2022). Mhd williamson nanofluid fluid flow and heat transfer past a non-linear stretching sheet implanted in a porous medium: effects of heat generation and viscous dissipation. *Processes*, 10(6), 1221. https://doi.org/10.3390/pr10061221

[12] M. Bibi, M. Malik, & A. Zeeshan. (2019). Numerical analysis of unsteady magneto-biphase williamson fluid flow with time dependent magnetic field. *Communications in Theoretical Physics*, 71(2), 143. https://doi.org/10.1088/0253-6102/71/2/143

[13] T. Srinivasulu & B. S. Goud. (2021). Effect of inclined magnetic field on flow, heat and mass transfer of Williamson nanofluid over a stretching sheet. *Case Studies in Thermal Engineering*, 23, 100819. https://doi.org/10.1016/j.csite.2020.100819

[14] C. Reddy, F. Ali, B. Mahanthesh, & N. Kishan. (2021). Irreversibility analysis of radiative heat transport of williamson material over a lubricated surface with viscous heating and internal heat source. *Heat Transfer*, 51(1), 395-412. https://doi.org/10.1002/htj.22312

[15] T. Hayat, Y. Saeed, S. Asad, & A. Alsaedi. (2015). Soret and dufour effects in the flow of williamson fluid over an unsteady stretching surface with thermal radiation. *Zeitschrift Für Naturforschung A*, 70(4), 235-243. https://doi.org/10.1515/zna-2014-0252

[16] M. Akolade, T. Oyekunle, H. Momoh, & M. Awad. (2022). Thermophoretic movement, heat source, and sink influence on the williamson fluid past a riga surface with positive and negative soret-dufour mechanism. *Heat Transfer*, 51(5), 4228-4246. https://doi.org/10.1002/htj.22497

[17] R. Choudhari. (2024). Integrated analysis of electroosmotic and magnetohydrodynamic peristaltic pumping in physiological systems: implications for biomedical applications. *Zamm - Journal of Applied Mathematics and Mechanics*, 104(8). https://doi.org/10.1002/zamm.202400163

[18] M. T. d. Araujo, L. J. d. S. Furlan, A. C. Brandi, & L. F. d. Souza. (2022). A semi-analytical method for channel and pipe flows for the linear phan-thien-tanner fluid model with a solvent contribution. *Polymers*, 14(21), 4675. https://doi.org/10.3390/polym14214675

[19] E. Karabut, A. Petrov, & E. Zhuravleva. (2018). Semi-analytical study of the Voinov's problem. *European Journal of Applied Mathematics*, 30(2), 298-337. https://doi.org/10.1017/s0956792518000098

[20] D. Al-Bogami, D. Maturi, & H. Alshehri. (2023). Adomian decomposition method for solving fractional time-klein-gordon equations using maple. *Applied Mathematics*, 14(06), 411-418. https://doi.org/10.4236/am.2023.146024

[21] N. Das. (2019). Study of properties of differential transform method for solving the linear differential equation. *Asian Journal of Engineering and Applied Technology*, 8(2), 50-56. https://doi.org/10.51983/ajeat-2019.8.2.1138

[22] J. Iqbal, K. Shabbir, & L. Guran. (2022). Stability analysis and computational interpretation of an effective semi analytical scheme for fractional order non-linear partial differential equations. *Fractal and Fractional*, 6(7), 393. https://doi.org/10.3390/fractalfract6070393

[23] A. Khan, S. Ullah, K. Shah, M. Alqudah, T. Abdeljawad, & F. Ghani. (2023). Theory and semi-analytical study of micropolar fluid dynamics through a porous channel. *Computer Modeling in Engineering & Sciences*, 136(2), 1473-1486. https://doi.org/10.32604/cmes.2022.023019

[24] S. Khirsariya & S. Rao. (2023). On the semi-analytic technique to deal with nonlinear fractional differential equations. *Journal of Applied Mathematics and Computational Mechanics*, 22(1), 17-30. https://doi.org/10.17512/jamcm.2023.1.02

[25] C. Ma. (2019). A novel computational technique for impulsive fractional differential equations. *Symmetry*, 11(2), 216. https://doi.org/10.3390/sym11020216

[26] O. Odetunde. (2021). Error estimation for differential transform method (dtm)solution of non-linear siqrm biological model. *Journal of Fundamental and Applied Sciences*, 13(3), 1327-1339. https://doi.org/10.4314/jfas.v13i3.12

[27] M. Shams, N. Kausar, K. Alayyash, M. Al-Shamiri, N. Arif, & R. Ismail. (2023). Semi-analytical scheme for solving intuitionistic fuzzy system of differential equations. *IEEE Access*, 11, 33205-33223. https://doi.org/10.1109/access.2023.3241482

[28] P. Vimala & P. Omega. (2018). Differential transform method in general orthogonal curvilinear coordinates. *Journal of Informatics and Mathematical Sciences*, 10(1-2), 271-278. https://doi.org/10.26713/jims.v10i1-2.1052

[29] D. Walter, H. Fichtner, & Y. Litvinenko. (2021). A perturbative approach to a nonlinear advection-diffusion equation of particle transport., 139. https://doi.org/10.22323/1.395.0139

[30] A. S. Kelil & A. R. Appadu. (2020). On semi-classical orthogonal polynomials associated with a modified sextic freud-type weight. *Mathematics*, 8(8), 1250. https://doi.org/10.3390/math8081250

[31] C. Y. Wang. (1989). Free convection on a vertical stretching surface. *ZAMM-Journal of Applied Mathematics and Mechanics/Zeitschrift für Angewandte Mathematik und Mechanik*, 69(11), 418-420. https://doi.org/10.1002/zamm.19890691115

[32] R. S. Gorla & I. Sidawi. (1994). Free convection on a vertical stretching surface with suction and blowing. *Applied Scientific Research*, 52, 247-257. https://doi.org/10.1007/BF00853952

[33] W. A. Khan & I. Pop. (2010). Boundary-layer flow of a nanofluid past a stretching sheet. *International Journal of Heat and Mass Transfer*, 53(11-12), 2477-2483. https://doi.org/10.1016/j.ijheatmasstransfer.2010.01.032

[34] S. Alao, R. A. Oderinu, E. I. Akinola, & O. E. Opaleye. (2022). An alternative method for investigating the effect of squeezing flow of a Casson fluid between parallel walls on magnetic field. *Journal of Mathematical and Computational Science*, 12, 1-12.